Multi-Threshold Inertial Switch With Acceleration Direction Detection Capability

Multi-threshold Inertial Switch with Acceleration Direction Detection Capability

*Qiu Xu, Lvjun Wang and Mohammad I. Younis**

***Abstract*—We present an inertial switch with three threshold levels, which can provide quantitative acceleration measurements and detect the acceleration direction in the x-y plane. The designed device has four movable electrodes attached to the proof mass (one at every side of the square proof mass) and 12 flexible stationary electrodes (three on each side). When the device is subjected to an acceleration input, the movable electrode can contact one or more of the 12 stationary electrodes based on the acceleration magnitude and direction. The acceleration direction can be determined by identifying the individual electrical switches that are activated. The designed switch is simulated using a finite element model under different acceleration signals of various magnitudes and directions. A device prototype has been fabricated using the SOIMUMPs process and has been tested by a drop-table system under various shock accelerations in different directions. The experimental and simulation results show good agreement indicating that the acceleration direction detection accuracy and resolution improve with the increase in the number of used electrical switches.**

***Index Terms*—Acceleration direction detection, inertia sensor, MEMS, multi-threshold**

I. INTRODUCTION

CONSIDERABLE research has been directed recently for microelectromechanical systems (MEMS) inertial microswitches due to the rapid development of portable gadgets, handheld devices, and wearable technologies, combined with the emerging applications in sport, military, and automotive sectors. This is due to the attractive features of these switches, compared to the conventional mechanical inertial microswitches, which include zero power consumption at normal state, low cost, compact size, and large volume production [1-11]. These switches are increasingly proposed to be used in various civilian and military fields, transportation, automobiles safety, healthcare, and safety-and-arming systems. With the emergence of the internet of things (IoT), MEMS inertial switches offer significant advantages due to their low power consumption that allow them to be deployed in remote areas and hard-to-be-powered applications.

An inertial switch is considered a passive device that consumes no power unless it is affected by an acceleration signal above certain threshold. It can provide substantial benefits in saving energy compared to accelerometers, which continuously consume power even if not affected by acceleration inputs. Therefore, the inertial switch is a suitable option to be used and integrated in systems where energy consumption is a critical concern [12-15].

The majority of the reported inertial switches have a single acceleration threshold, so that they only provide ON-OFF information [16-22]. They produce ON signal if the acceleration is higher than the predesignated threshold level and OFF signal otherwise. However, for some applications, there is a need for quantitative information about the experienced acceleration, such as for brain impact injuries to classify the injury as mild, severe, etc. Niyazi et al. [23] presented a bidirectional inertial switch with two threshold levels. Reddy et al. [24] reported an inertial switch with 10 threshold levels, which can sense the acceleration between 20g and 250g. However, these designs can only detect the magnitude of acceleration in one or two directions. Xu et al. [25] proposed a shock sensor that can detect the acceleration with a range from 800g to 2600g with three threshold levels in the ±x and ±y axes.

As discussed, the majority of research has been focused on classifying the magnitude of acceleration; however, few research has been directed toward identifying the acceleration direction despite its importance. In many applications, such as in military, automotive, healthcare, and industry, it is essential to detect the acceleration direction [26-29]. One common way of detecting the magnitude and direction of the applied acceleration is by using a combination of multiple (two or three) uniaxial accelerometers with orthogonal axes or multi-axis accelerometers like in Inertial Measuring Unit (IMU). However, using these units adds to the complexity, size, and cost of the total system [26, 30]. Thus, it is of great importance to design an inertial switch for detecting the acceleration direction. In a recent work, Xi et al. [26] reported an inertial switch with a single threshold level, which is capable of detecting impact direction in 3D space. It cannot however provide the direction of acceleration accurately, but rather can determine the approximate intervals between acceleration directions. In addition, these intervals may have an overlapping range.

Manuscript received Month xx, 2xxx; revised Month xx, xxxx; accepted Month x, xxxx. This work was supported in part by King Abdullah University of Science and Technology (KAUST). The authors acknowledge the help of Mr. Raed Alahmdi in fabricating the test fixtures and rotary disk and Dr. Rodrigo Rocha for bonding the printed circuit board. (Corresponding author: Mohammad I. Younis).

The authors are with the Physical Sciences and Engineering Division, King Abdullah University of Science and Technology, Thuwal, 23955-6900, Saudi Arabia. (e-mail: qiu.xu@kaust.edu.sa, lvjun.wang@kaust.edu.sa, Mohammad. Younis@kaust.edu.sa)

In this work, we propose a low-power multi-threshold MEMS inertia sensor with the capability of detecting acceleration direction at higher resolution. With the presented device, acceleration in all axes can be sensed, which can work bidirectionally for each axis.

II. PHYSICAL MODEL AND WORKING PRINCIPLE

A. Structure Design and Theoretical Analysis

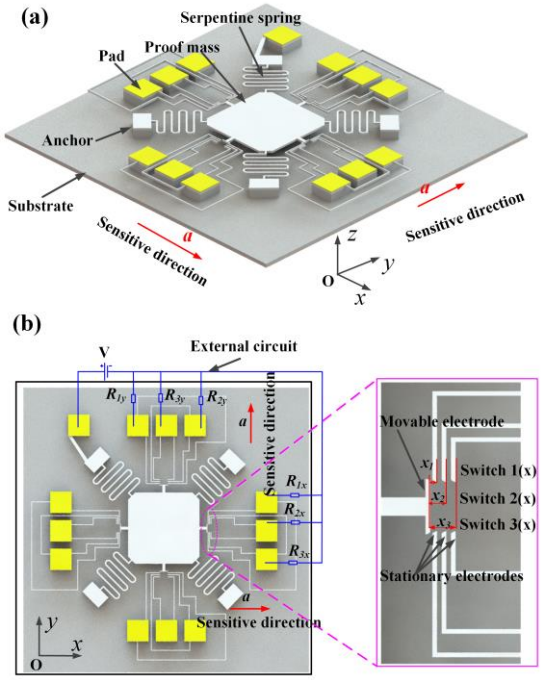

Fig.1 (a) A 3D sketch of the designed multi-threshold inertial micro-switch. (b) Top view of the designed switch with a schematic showing the switches.

Fig.1 (a) illustrates the designed inertial switch with three threshold levels. The designed device is mainly composed of three parts: the proof mass suspended by four springs, four movable electrodes (one at every side of the square proof mass), and twelve stationary electrodes (one group of three at each side). The designed inertial switch is bidirectional that can detect acceleration in all axes. Fig. 1(b) depicts the movable electrode and stationary electrodes 1, 2, and 3 that corresponds to the first, second, and third acceleration thresholds. In addition, the gaps separating the flexible and stationary electrodes x_1, x_2, x_3 are 5μm, 12μm, and 20μm, respectively.

Next, we assume that the inertial switch undergoes a half-sinusoidal wave acceleration $a(t)$ with amplitude a_0 and pulse width t_0 in an arbitrary direction (θ) in the x-y plane, Fig. 2. Ignoring damping for simplicity, the equations of motion can be expressed as:

$$m\ddot{x} + k_x x = ma(t)\cos(\theta) \qquad (1)$$

$$m\ddot{y} + k_y y = ma(t)\sin(\theta) \qquad (2)$$

where m is the equivalent mass of the proof mass, x, y are the relative displacement of the proof mass and substrate in the x and y axis, respectively, and k_x and k_y are the spring constants in x and y axis, respectively.

When any acceleration component in x and/or y directions applied to the device exceeds the predesignated threshold levels a_{th1}, a_{th2}, and a_{th3}, the movable electrode will contact the corresponding stationary electrode 1, 2, and 3 in x and/or y directions, forming an electrical path and generating a trigger signal.

Solving Eqs. (1) and (2) yields [31]:

$$x(t) = \frac{a_0\cos\theta}{(k_x/m)-(\pi/t_0)^2}\left[\sin\frac{\pi}{t_0}t - \frac{\pi}{\sqrt{k_x/mt_0}}\sin\sqrt{\frac{k_x}{m}}t\right] \qquad (3)$$

$$y(t) = \frac{a_0\sin\theta}{(k_y/m)-(\pi/t_0)^2}\left[\sin\frac{\pi}{t_0}t - \frac{\pi}{\sqrt{k_y/mt_0}}\sin\sqrt{\frac{k_y}{m}}t\right] \qquad (4)$$

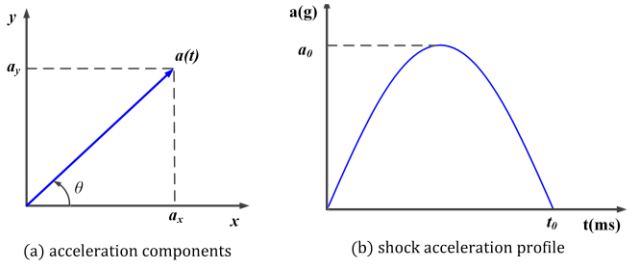

(a) acceleration components (b) shock acceleration profile

Fig. 2. Applied acceleration: (a) direction, and (b) profile over time.

The dynamic response of the switch is suppressed when the ratio t_0/T_{nat} is smaller than 0.5 according to the shock-response spectrum (SRS) [25]. Here, t_0 and T_{nat} represent the pulse width of the shock pulse and the natural period of the system, respectively. When t_0/T_{nat} is within the interval of $0.5< t_0/T_{nat} <4.0$, the response experiences large amplification. It is worth noting that the peak amplification factor (the dynamic amplitude A_{dyn} normalized to the static amplitude A_{sta}) is 1.76 when $t_0/T_{nat} \approx 0.8$. For $t_0/T_{nat} > 4$, the response becomes less sensitive to the pulse width (quasi-static regime). Here the amplification factor becomes close to unity.

B. Measurement of Acceleration Direction

1. Working principle of the inertial switch with one threshold

For simplicity, we first study the operation principle of the biaxial inertial switch assuming a single threshold value. As shown in Fig. 3, there is a total of 8 contact-electrodes in two states when the acceleration in different directions applied to the device. Electrode 1(x) and electrode 1(y) represent the first stationary electrodes in the +x and +y directions. When subjected to an acceleration signal, there are two possible scenarios: the proof mass can contact a single electrode (e.g., electrode 1(x)) or the proof mass can contact two adjacent electrodes simultaneously (e.g., electrode 1(x) and electrode 1(y)). It is obvious that each contact-electrode indicates a certain interval of the acceleration direction. Therefore, the acceleration direction interval can be detected depending on the switches that make contact.

Note that the critical angle values of interval limits (θ_1, θ_2, and θ_3) change with the amplitude of the acceleration. For simplicity, here we only discuss a case study of acceleration magnitude ($1.5a_{th1}$), where a_{th1} is the first threshold acceleration in switch 1(x) and switch 1(y). The first quadrant of the x-y plane can be divided into three intervals.

(a) When the inertial switch is subjected to $a(t)$ at θ=0, the proof mass only contacts electrode 1(x) as illustrated

in Fig. 3(a).

(b) Applying $a(t)$ at $\theta=\theta_1$ as shown in Fig. 3(b) makes the proof mass start to contact electrode 1(y) while keeping contact with electrode 1(x). It can be concluded that when the proof mass only contacts electrode 1(x), the acceleration direction θ is in the interval of $0\leq\theta<\theta_1$.

(c) Under $a(t)$ at $\theta=\theta_2$, Fig. 3(c), the proof mass is no longer in contact with electrode 1(x), but it keeps contact with electrode 1(y). When the proof mass contacts the two electrodes adjacently (electrode 1(x) and electrode 1(y)) simultaneously, it indicates that $a(t)$direction θ is in the interval of $\theta_1\leq\theta\leq\theta_2$, Fig. 3(b), Fig. 3(c).

(d) Fig. 3(d) shows that the proof mass only contacts the single electrode 1(y) under $a(t)$ at θ=90°.

When the inertial switch is subjected to $a(t)$ at θ=0, the proof mass only contacts electrode 1(x) as illustrated in Fig. 3(a). Applying $a(t)$ at $\theta=\theta_1$ as shown in Fig. 3(b) makes the proof mass start to contact electrode 1(y) while keeping contact with electrode 1(x). It can be concluded that when the proof mass only contacts electrode 1(x), the acceleration direction θ is in the interval of $0\leq\theta<\theta_1$. Under $a(t)$ at $\theta=\theta_2$, Fig. 3(c), the proof mass is no longer in contact with electrode 1(x), but it keeps the contact with electrode 1(y). When the proof mass is contact with the two electrodes adjacently (electrode 1(x) and electrode 1(y)) simultaneously, it indicates that $a(t)$direction θ is in the interval of $\theta_1\leq\theta\leq\theta_2$, Fig. 3(b), Fig. 3(c). Fig. 3(d) shows that the proof mass only contacts the single electrode 1(y) under $a(t)$ at θ=90°. Therefore, when the proof mass touches electrode 1(y) only, θ is in the interval of $\theta_2<\theta\leq$90°. The same principle applies for an acceleration input in the direction in the second, third, and fourth quadrants of the x-y plane. Table I summarizes the corresponding relationship between contact-electrodes and the acceleration direction interval for the four quadrants.

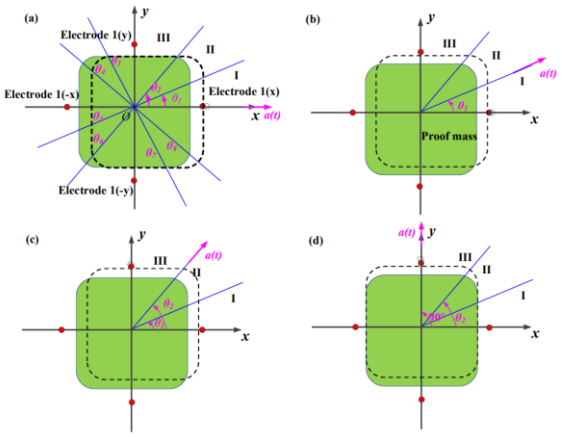

Fig. 3. Working principle of the inertial switch with a single threshold value: (a) The proof mass only contacts a single electrode 1(x) at θ=0. (b) The proof mass still touches electrode 1(x) and just begins to contact electrode 1(y) at $\theta=\theta_1$. (c) The proof mass just loses contact with electrode 1(x) at $\theta=\theta_2$. (d) The proof mass touches electrode 1(y) at θ=90°. The green squares and the red circles are the original locations, while the dashed squares and the dashed circles are the new locations.

TABLE I

CONTACT-ELECTRODES AND THE CORRESPONDING ACCELERATION DIRECTION INTERVALS WHEN THE DEVICE IS SUBJECTED TO AN ACCELERATION INPUT IN THE X-Y PLANE, FIG. 3.

Number	Contact-electrodes	Acceleration direction interval θ
1	1(x)	$\theta_8<\theta<\theta_1$
2	1(x), 1(y)	$\theta_1\leq\theta\leq\theta_2$
3	1(y)	$\theta_2<\theta<\theta_3$
4	1(y),1(-x)	$\theta_3\leq\theta\leq\theta_4$
5	1(-x)	$\theta_4<\theta<\theta_5$
6	1(-x), 1(-y)	$\theta_5\leq\theta\leq\theta_6$
7	1(-y)	$\theta_6<\theta<\theta_7$
8	1(-y),1(x)	$\theta_7\leq\theta\leq\theta_8$

2. Working principle of the inertial switch with two thresholds

For brevity, we will focus here in the interval of 0°≤θ≤90°. As shown in Fig. 4, when subjecting the device to acceleration inputs with different directions in the first quadrant, there are a total of five contact-electrodes in five states. Electrode 2(x) and electrode 2(y) represent the second stationary electrodes in the +x and +y direction, respectively.

(a) Fig. 4(a) shows that the proof mass passes through electrode 1(x) and contacts electrode 2(x) under $a(t)$ at θ=0.

(b) As shown in Fig. 4(b), the proof mass just starts to contact electrode 1(y) when the acceleration at $\theta=\theta_9$ is applied to the inertial switch. Therefore, the acceleration direction θ is in the interval of $0\leq\theta<\theta_9$ when the proof mass passes by electrode 1(x) and contacts electrode 2(x).

(c) Applying $a(t)$ at $\theta=\theta_{10}$ in Fig. 4(c), the proof mass just begins to contact electrode 2(y). Therefore, when the proof mass touches electrode 1(x), electrode 2(x), and electrode 1(y) instead of electrode 2(y), θ must be in the interval of $\theta_9\leq\theta<\theta_{10}$.

(d) Fig. 4(d) illustrates that the proof mass just loses contact with electrode 2(x) under $a(t)$ at $\theta=\theta_{11}$. Therefore, when the four electrodes are contacted by the proof mass, the acceleration direction θ belongs to the interval of $\theta_{10}\leq\theta<\theta_{11}$.

(e) When the switch is subjected to $a(t)$ at $\theta=\theta_{12}$ as shown in Fig. 4(e), the proof mass just loses contact with electrode 1(x). The acceleration direction θ must be in the range of $\theta_{11}\leq\theta<\theta_{12}$ when the proof mass touches electrode 1(x), electrode 1(y), and electrode 2(y).

(f) Fig. 4(f) shows that the proof mass only contacts electrode 1(y) and electrode 2(y) under $a(t)$ at θ=90°. It indicates that θ is in the interval of $\theta_{12}\leq\theta\leq$90°.

The corresponding relationship between the contact electrodes and the acceleration direction intervals in the first quadrant can be summarized in Table II. Comparing Table I with Table II, it is concluded that for the inertial switch with a single threshold level the acceleration direction in the first quadrant is divided into three regimes (I, II, III). On the other hand, for the inertial switch with two threshold levels, the acceleration direction in the first quadrant is divided into five regimes (I, II, III, IV, V). With the increase of the threshold levels, the number of the contact-electrodes increases, and thus the resolution of the acceleration direction detection improves. The operation principle of the biaxial inertial switch with three thresholds is similar, and hence, for brevity, it will not be discussed here.

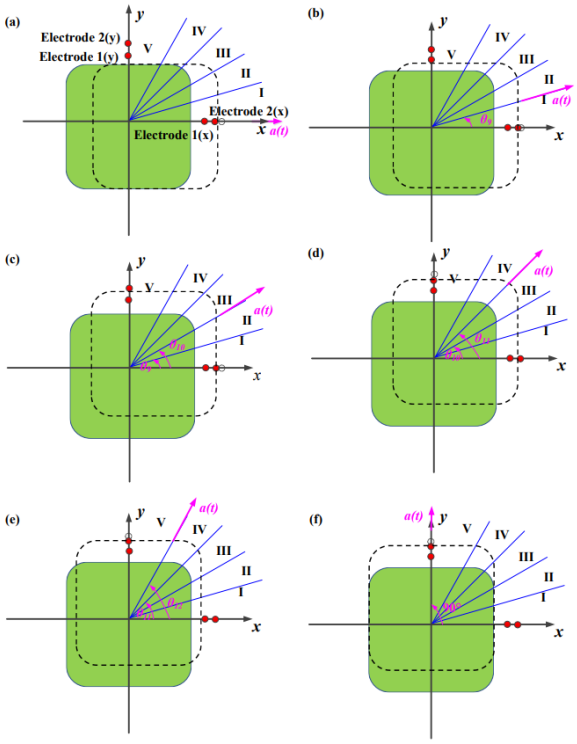

Fig. 4. Working principle of the inertial switch with two thresholds. The proof mass contacts different electrodes when subjected to a constant acceleration at various directions.

TABLE II
CONTACT-ELECTRODES THAT CORRESPONDS TO THE ACCELERATION DIRECTION INTERVALS IN THE FIRST QUADRANT FOR A TWO-THRESHOLD INERTIA SENSOR，FIG. 4.

Number	Contact-electrodes	Acceleration direction interval θ
1	1(x), 2(x)	$0 \le \theta < \theta_9$
2	1(x), 2(x), 1(y)	$\theta_9 \le \theta < \theta_{10}$
3	1(x), 2(x), 1(y), 2(y)	$\theta_{10} \le \theta < \theta_{11}$
4	1(x), 1(y), 2(y)	$\theta_{11} \le \theta < \theta_{12}$
5	1(y), 2(y)	$\theta_{12} \le \theta < 90°$

III. SIMULATION

The ANSYS software [32] is employed to conduct modal and dynamic finite-element (FE) analysis, including contact，for the designed inertial switch with three threshold levels as shown in Fig. 5. The element type of SOLID 186 was chosen to mesh the mass-spring model utilizing the SWEEP method, where the end sections of three stationary electrodes (corresponding to the first, second, and third threshold acceleration) and the suspended springs far away from the proof mass are set to a fixed constraint. The contact element types are TARGE170 and CONTA174. Here the contact pairs are defined by the lateral surface of the moveable electrode and the three stationary electrodes. The properties of silicon [16] are the below: Young's modulus, Poisson's ratio and density are 130GPa, 0.23, and 2.33 g·cm^{-3}, respectively.

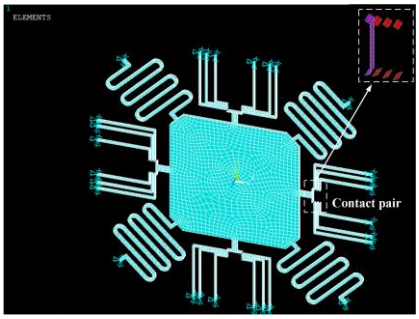

Fig. 5. The ANSYS finite-element model of the inertial switch with three thresholds and the corresponding contact pairs.

A. Modal Analysis

A finite element modal analysis is conducted to calculate the structure's natural frequencies. It can be seen from Fig. 6 that the first, second, third, and fourth natural frequencies are 4991Hz, 7048Hz, 7048Hz, and 10987 Hz, respectively. The first mode is in the z-direction as shown in Fig. 6(a). The second and third modes (Fig. 6b and Fig. 6c) have the same frequencies due to the symmetry in the design of the structure in the x and y directions. The fourth mode (Fig. 6d) rotates along the direction of the diagonal line of the proof mass.

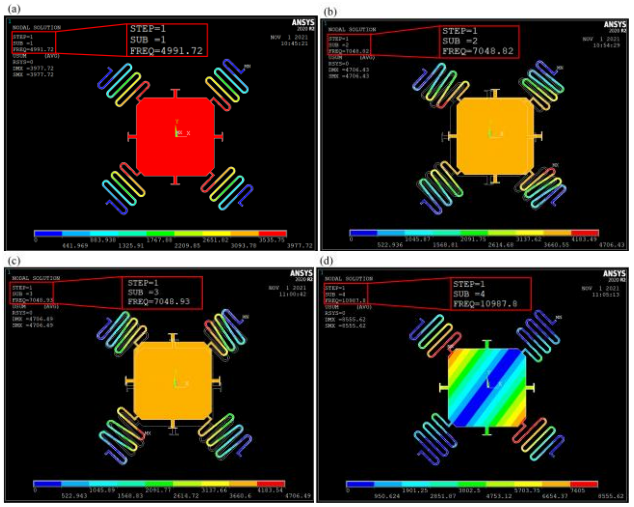

Fig. 6. First four mode shapes of the designed biaxial inertial switch. (a) First mode. (b) Second mode. (c) Third mode. (d) Fourth mode.

B. Simulation of the Dynamic Response

Fig.7 shows the simulated curves of the x-axis and y-axis displacement over time of the movable electrode under an acceleration of 1350g-0.5ms at different directions in the x-y plane. As shown in Fig. 7(a-b), only the maximum x-axis displacement is greater than the electrode 1(x) gap x_1 under the acceleration at 0 and 30°, and the proof mass only contacts electrode 1(x). Generally, the acceleration that makes the proof mass just touching the stationary electrode is defined as the threshold acceleration. It can be seen from Fig. 7(c) that the y-axis displacement is just equal to the electrode 1(y) gap y_1 under the acceleration 1350g-0.5ms at 40.81°. It indicates that the threshold acceleration component in the y-axis is 845g, but the designed switch 1(y) most probably will not be triggered because the contact time is not enough for switching. When the

proof mass touches electrode 1(x) only, this means that the acceleration direction θ belongs to the interval of $0°\leq\theta\leq40.81°$. As shown in Fig. 7(d), the x-axis and y-axis displacements are on top of each reaching beyond the electrode 1 gap x_1 or y_1, which indicates that the proof mass contacts electrode 1(x) and electrode 1(y) simultaneously. Fig. 7(e) shows that the proof mass contacts electrode 1(y) and just starts to lose contact with electrode 1(x). Based on Fig. 7s (c-e), the acceleration direction θ belongs to $40.81°<\theta<49.19°$ when both switch 1(x) and switch 1(y) are activated. Fig. 7(f) shows that only switch 1(y) is activated. So, the acceleration direction θ belongs to $49.19°\leq\theta\leq90°$ when the proof mass only contacts electrode 1(y). Table III lists the simulation results of the switch state, acceleration digital output, and acceleration direction interval in the first quadrant in the x-y plane.

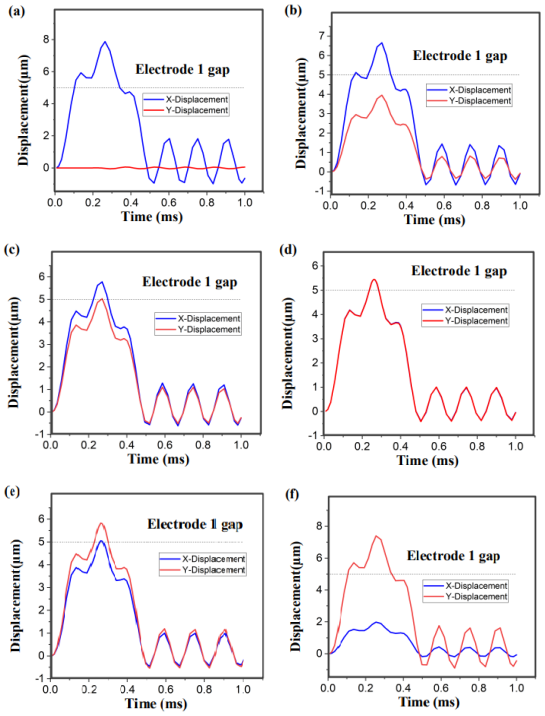

Fig. 7. Dynamic response of the multi-threshold inertial switch under the applied acceleration with the amplitude of 1350g and pulse width of 0.5ms at different directions in the x-y plane: (a) θ=0°, (b) θ=30°, (c) θ=40.81°, (d) θ=45°, (e) θ=49.19°, (f) θ=75°.

TABLE III
SIMULATED CONTACT-ELECTRODES CORRESPONDING TO THE INTERVAL OF THE ACCELERATION DIRECTION WHEN THE DEVICE IS SUBJECTED TO THE ACCELERATION WITH THE AMPLITUDE OF 1350G AND DURATION OF 0.5MS.

Number	Contact-electrodes	Acceleration direction θ (°)
1	1(x)	$0\leq\theta\leq40.81°$
2	1(x), 1(y)	$40.81°<\theta<49.19°$
3	1(y)	$49.19°\leq\theta\leq90°$

As the applied acceleration increases, the proof mass contacts not only electrode 1 but also electrode 2. Fig. 8 demonstrates the simulated displacement of the proof mass as a function of time for the case of applying an acceleration of 3000g amplitude at directions of 0, 17.9°, 30°, 43.89°, 46.11°, 55°, 72.1° and 90°. Table IV provides the acceleration direction interval in the first quadrant in the x-y plane. For the inertial switch with a single threshold acceleration, the acceleration direction is divided into three intervals as shown in Table III. However, for the switch with two thresholds, the acceleration direction is divided into five intervals as shown in Table IV. It indicates that the acceleration direction of the latter is more accurate than the former. As the threshold levels increase (i.e., three-threshold inertial switch), the accuracy of acceleration direction increases.

TABLE IV
SIMULATED CONTACT-ELECTRODES CORRESPONDING TO THE INTERVAL OF THE ACCELERATION DIRECTIONS WHEN THE ACCELERATION AMPLITUDE IS 3000G-0.5MS APPLIED ON THE DESIGNED INERTIAL SWITCH.

Number	Contact-electrodes	Acceleration direction interval θ (°)
1	1(x), 2(x)	$0\leq\theta< 17.9°$
2	1(x), 2(x), 1(y)	$17.9°\leq\theta<43.89°$
3	1(x), 2(x), 1(y), 2(y)	$43.89°\leq\theta<46.11°$
4	1(x), 1(y), 2(y)	$46.11°\leq\theta<72.1°$
5	1(y), 2(y)	$72.1°\leq\theta\leq90°$

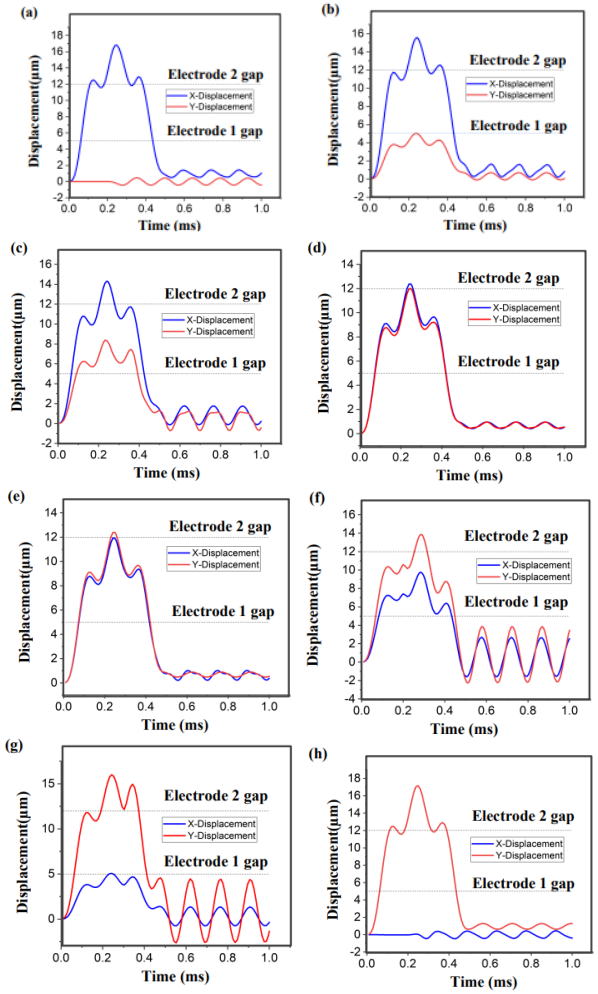

Fig. 8. Simulated movable electrode displacement in the time domain under the input acceleration with the amplitude of 3000g and pulse width of 0.5ms at different acceleration directions: (a) θ=0°, (b) θ=17.9°, (c) θ=30°, (d) θ=43.89°, (e) θ=46.11°, (f) θ=55°, (g) θ=72.1°, (f) θ=90°.

IV. CHARACTERIZATION

Fig. 9 shows the inertial switch fabricated by MEMSCAP based on Silicon-On-Insulator Multi-User MEMS process (SOIMUMPs). The high contact resistance is due to the poor conductivity of silicon material. Therefore, it is essential to

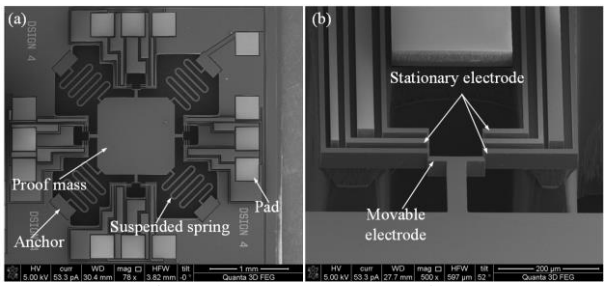

Fig. 9. SEM images of the prototype devices. (a) The fabricated inertial switch with three threshold levels. (b) Three-dimensional view of the stationary electrodes and the movable electrode.

sputter a Cr/Cu layer with appropriate thickness (about 200 nm) on these fabricated devices to enhance the electric conductivity and improve the quality of the trigger signal. The appropriate thickness of the Cr/Cu layer does not cause short circuit between adjacent pads, nor between the substrate and device layers due to undercuts in the oxide layer, which make them electrically isolated from each other.

A. Latching Circuit for Detecting the Acceleration Direction

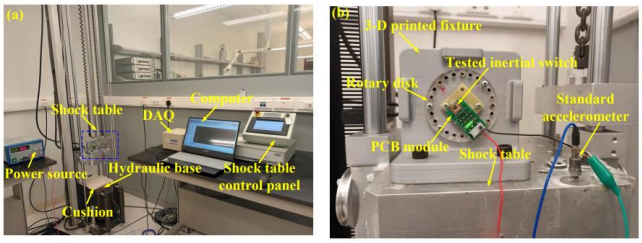

Fig. 10. (a) The drop table test system setup. (b) A close-up of the shock table and PCB module.

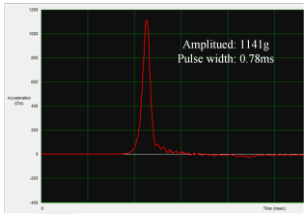

Fig. 11. Example of the generated half-sine acceleration signal from a drop-table test with a peak acceleration of 1141g and a pulse width of 0.78ms.

Fig. 10(a) shows that he fabricated prototype devices were tested by a drop-table system. The accelerometer ADXL-193 with a sensitivity of 8mV/g was used as a reference. In this experiment, a power source (8V) was connected to the latching circuit on the PCB module in Fig. 10(b), where the latching circuit was used to observe if the LED lights up or not. Thus, the direction of acceleration can be determined by which LED lights up.

The shock table was lifted to pre-determined heights *H* by the hoist. It generates half-sine wave acceleration signals with different magnitudes when the shock table freely dropped onto the base platform from various pre-set heights *H*. The amplitude of acceleration increases with the height H. For example, Fig. 11 demonstrates that a shock pulse of magnitude 1141g and duration 0.78ms is generated by the shock table system when the drop table was released freely from the pre-determined height of 20cm.

Here, we firstly demonstrate an approach to capture the switching action based on a latching circuit. The latching circuit is attached to a PCB module with eight LEDs lights, as shown in Fig. 12(a), which can lead to higher resolution results. The latching circuit mainly consists of eight LEDs, a control reset, and eight resistances. The working principle of the latching circuit is as follows: It can be seen from Fig. 12(b) that two terminals of the inertial switch are connected to a 5V power supply and the control line (C) of the latching circuit. The data line (D) of the latch is high and the control line (C) is low on standby. When the switch is triggered, a pulse signal with microseconds duration is generated and then acquired by the control input (C). The output (Q) indicated by LED 1 is then latched to high state (lights up). When the PCB is subjected to a sufficient acceleration, the movable electrode moves toward the stationary electrode and touches it. Therefore, the corresponding inertial switch (e.g. switch 1(x)) is triggered and the corresponding LED turns on. Note that the LED is still in the ON state even if the movable electrode loses contact with the stationary electrode, which is very similar to the trigger signal captured by the multi-channel oscilloscope.

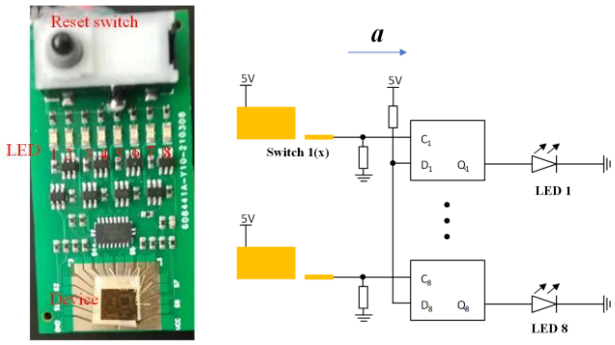

(a) (b)

Fig. 12 (a) An image of the latching circuit. (b) A schematic outline of the latching circuit.

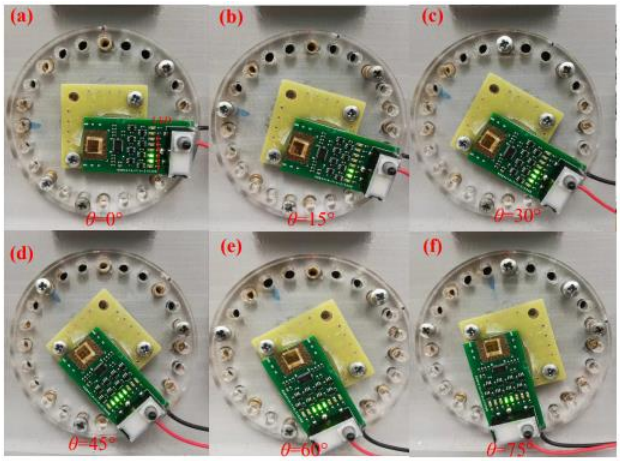

Fig. 13. The testing PCB platform with the fabricated MEMS multi-threshold inertial microswitch showing its orientation for inducing acceleration at different directions under 3000g.

The PCB with fabricated inertial microswitch is used to monitor acceleration direction. Testing has been done for the PCB module with the fabricated inertial microswitch undergoing different acceleration directions. As shown in Fig. 13, the fabricated device was applied by the acceleration of 3000g at θ=0°,15°,30°,45°,60°,75° in the x-y plane, respectively. LED 1, LED 2, LED 3, LED 4, LED 5 and LED 6 represent the trigger signal of switch 3(x), switch 2(x), switch 1(x), switch 1(y), switch 2(y), and switch 3(y), respectively. It can be seen from Figs. 13(a-c) that only LED 2 and LED 3 turn on at θ<30° in the x-y plane, i.e., only switch 2(x) and switch 1(x) are triggered. When the acceleration direction belongs to the interval 15°<θ<45°, LED 2, LED 3 and LED 4 are in the ON state. LED 2, LED 3, LED 4 and LED 5 light up under the acceleration at θ=45° in the x-y plane. LED 2 turns off at θ=60° in the x-y plane. LED 3 also turns off at θ=75° in the x-y plane. The relationship between the acceleration direction and LED state (ON/OFF) in the x-y planed is provided in Table V.

TABLE V
LED STATE CORRESPONDING TO THE MEASURED ACCELERATION DIRECTION INTERVALS UNDER THE ACCELERATION OF 3000G. LED STATE REPRESENT WHICH SWITCH IS TRIGGERED.

Number	LED 2 state	LED 3 state	LED 4 state	LED 5 state	Acceleration direction interval θ(°)
1	ON	ON	OFF	OFF	0°<θ< 30°
2	ON	ON	ON	OFF	15°<θ<45°
3	ON	ON	ON	ON	30°<θ<60°
4	OFF	ON	ON	ON	45°<θ<75°
5	OFF	OFF	ON	ON	60°<θ<90°

Fig. 14 demonstrates LED state under the acceleration of 4200g at θ=0°,15°,30°,45°,60°,75° and 90° in the x-y plane. LED 1, LED 2, LED 3, LED 4, LED 5 and LED 6 stands for the contact signal of switch 3(x), switch 2(x), switch 1(x), switch 1(y), switch 2(y), and switch 3(y), respectively. As shown in Fig. 14(a), LED1, LED 2 and LED 3 turn on at θ=0°, i.e., switch 1(x), switch 2(x) and switch 3(x) are activated. When the device is subjected to an acceleration of 4200g at θ=15°, LED 4 starts to turn on, which is illustrated in Fig. 14(b). Therefore, the acceleration direction belongs to the interval 0°<θ<15° when only LED 1, LED 2 and LED 3 are in the ON state. The other experimental results are summarized in Table VI.

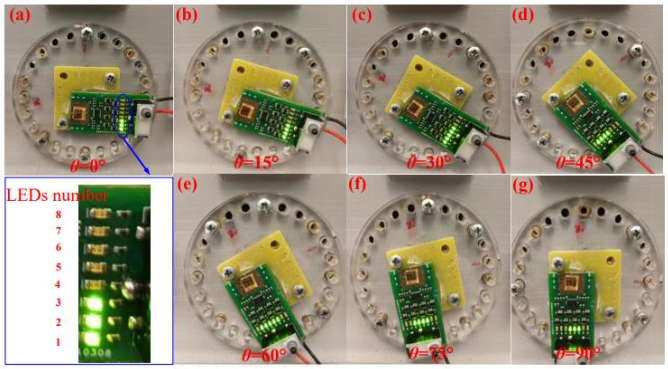

Fig. 14. The testing PCB with LEDs showing the switch's direction when subjected to an acceleration of 4200g at different directions.

TABLE VI
LED STATE CORRESPONDING TO THE EXPERIMENTAL ACCELERATION DIRECTION INTERVALS WHEN SUBJECTED THE ACCELERATION OF 4200G. LEDS STATE CAN BE DETERMINED BY WHICH CONTACT SWITCH TOUCHES.

Number	LED 1 state	LED 2 state	LED 3 state	LED 4 state	LED 5 state	LED 6 state	Acceleration direction interval θ(°)
1	ON	ON	ON	OFF	OFF	OFF	0°≤θ< 15°
2	ON	ON	ON	ON	OFF	OFF	0°<θ<30°
3	ON	ON	ON	ON	ON	OFF	15°<θ<45°
4	OFF	ON	ON	ON	ON	OFF	30°<θ<60°
5	OFF	ON	ON	ON	ON	ON	45°<θ<75°
6	OFF	OFF	ON	ON	ON	ON	60°<θ<90°
7	OFF	OFF	OFF	ON	ON	ON	75°<θ≤90°

B. Acceleration Direction Detection Based on the Multi-channel Oscilloscope

As shown in Fig. 15, the fabricated prototype devices were tested by a drop-table system in order to detect the acceleration direction based on the multi-channel oscilloscope, where the oscilloscope (Agilent 6000 MSO6034A) was used to capture the trigger signals. In this test, the inertial switch was associated with a power source (8V) and four voltage divider resistances (R_{1x}, R_{2x}, R_{1y}, and R_{2y}) of 330Ω. If the acceleration applied to the inertial microswitch was greater than the first, second, third threshold level, the corresponding trigger signals (e.g. switch 1(x), 2(x), 3(x)) can be caught by the multi-channel oscilloscope simultaneously. Four color signals achieved by a multichannel oscilloscope are shown in the test results: the yellow signal and the green signal stands for the trigger signals of switch 1(x) and switch 1(y), respectively; the contact signals in switch 2(x) and switch 2(y) are represented by the blue and the red signals, respectively.

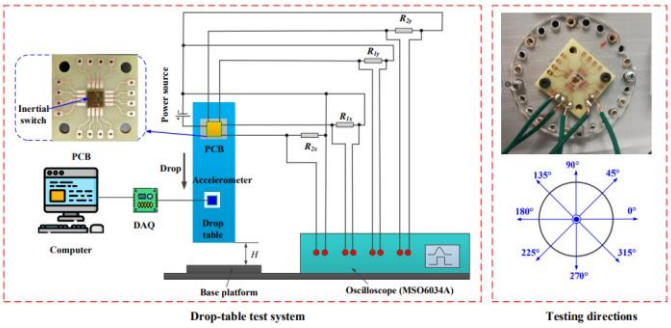

Fig. 15. The schematic diagram of testing circuit and the different testing directions.

1. Direction intervals of an inertial switch with a single threshold level

Here, the applied acceleration a is less than the second threshold acceleration a_{th2} but beyond the first threshold acceleration a_{th1}. Although the fabricated device is a multi-threshold inertial switch, the test is similar to testing the inertial switch with a single threshold level. By utilizing the method illustrated in Fig. 13, an acceleration signal of amplitude 1350 g was applied to the fabricated inertial switch at θ=0°, 15°, 30°, 45°, 75°, 90°. As shown in Fig.16(a-c), only the yellow trigger signal is visible under the acceleration with the

amplitude of 1350g at θ=0°,15°,30°. It indicates that only switch 1(x) is switched on. Fig. 16 (d) shows both the green and yellow signals. Therefore, both switch 1(x) and switch 1(y) are activated. Figs. 16(e-f) show only the green signal indicating the activation of switch 1(y) only.

TABLE VII
TEST RESULTS OF THE INERTIAL SWITCH: CONTACT-ELECTRODES CORRESPONDING TO THE DIRECTION RANGES OF ACCELERATION UNDER THE MEASURED ACCELERATION OF 1350G. 1(X) REPRESENTS THAT SWITCH 1(X) IS ON STATE.

Number	Contact-electrodes	Acceleration direction interval θ(°)
1	1(x)	0°<θ< 45°
2	1(x), 1(y)	30°<θ<75°
3	1(y)	45°<θ< 90°

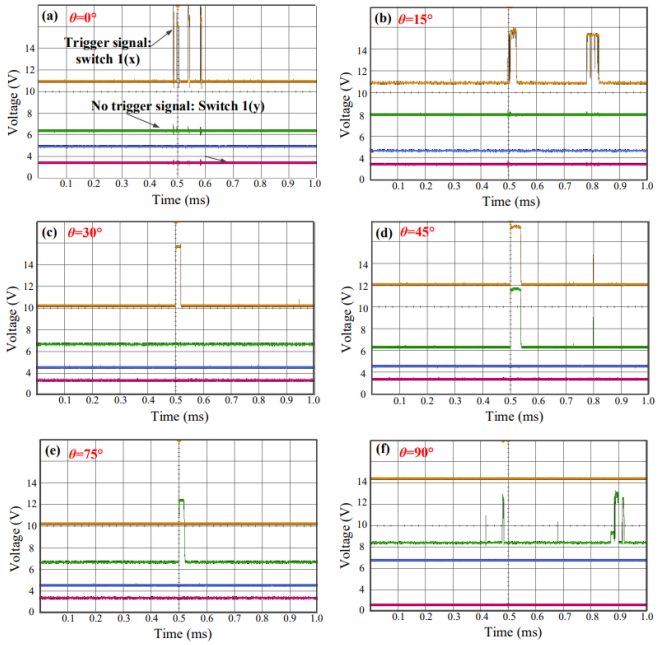

Fig. 16. Test results of the fabricated multi-threshold switch: the trigger signals under the acceleration of 1350g at different directions at θ=0°,15°,30°,45°,75°,90° in the x-y plane.

From the single threshold results we can conclude the following: (1) switch 1(x) is triggered only at $\theta \leq 30°$ in the x-y plane; (2) both switch 1(x) and switch 1(y) are triggered at θ=45°; (3) only switch 1(y) is activated at $\theta \geq 75°$ in the x-y plane. These results are summarized in Table VII. These results are in agreement with the relationship between contact electrodes corresponding to the acceleration direction intervals in Table I from the working principle of inertial switch with one threshold level. Also, they match well with those in Table III from simulations. The only difference between them is attributed to the fact that the tested acceleration direction can be only changed every 15° and is not continuous due to the experimental limitation in the current setup of the maximum possible number of holes on the circular plate as shown in Fig. 15.

2. Direction intervals of the inertial switch with two threshold levels

Here we test the inertial switch utilizing up to two threshold levels. Figs. 17(a-b) show the yellow trigger signal and the blue trigger signal. This implies that switch 1(x) and switch 2(x) are triggered. Fig. 17(c) shows the green trigger signal, which indicates that switch 1(y) is triggered as well. Fig. 17(d) shows all the four different colors indicating the activation of the four switches, switch 1(x), switch 2(x), switch 1(y), and switch 2(y). Fig. 17(e) shows that the blue signal disappeared indicating that switch 2(x) is OFF state. It can be seen from Fig. 17(f) that the yellow trigger signal also disappeared, which indicates that switch 1(x) is also OFF state. The test results are summarized in Table VIII. Comparing Table VII and Table VIII, the resolution of the detected acceleration direction interval improves with the increase of the threshold levels of the inertial switch. However, the demonstrated approach relying on a multi-channel oscilloscope is not practical for portable and compact systems and is limited by the number of channels/colors that the oscilloscope can offer (in our case four). Comparing Table V with Table. VIII, the method based on latching circuit is in good agreement. These experimental results in Table. VIII are basically in agreement with those in Table. II from working principle of the switch with two thresholds. Both of them can make the acceleration direction in the first quadrant divide into five regimes (1, 2, 3, 4, and 5).

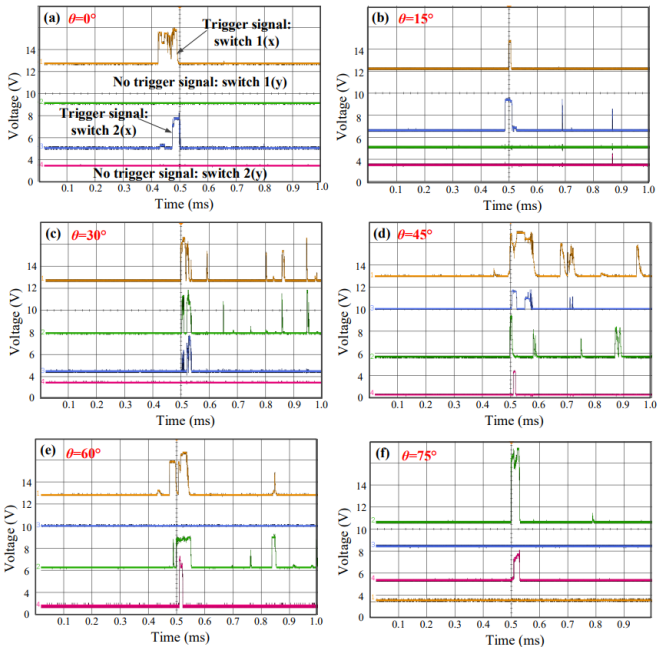

Fig. 17. Measurement results of the fabricated device utilizing two thresholds under a shock signal of amplitude 3000g at different directions θ=0°,15°,30°,45°,60°,75° in the x-y plane. The first testing threshold acceleration and the second testing threshold acceleration in switch 1(x) and switch 2(x) are 870g and 1982g, respectively.

In summary, comparing to the acceleration direction tested method based on the trigger signals captured by a multi-channel oscilloscope, the main advantage of the latching circuit is that we can design many LEDs, which can detect many trigger signals. And it provides a simpler output that can be read and

understood easily and without any external read-out mechanisms. Therefore, this method provides the ability to have higher number of bits compared to the oscilloscope that limits the number of bits due to the number of channels.

TABLE VIII
EXPERIMENTAL RESULTS OF THE FABRICATED INERTIAL SWITCH: CONTACT-ELECTRODES CORRESPONDING TO THE TESTED ACCELERATION DIRECTION INTERVALS. 1(x), 2(x) REPRESENT THAT SWITCH 1(x) AND SWITCH 2(x) ARE ACTIVATED.

Number	Contact-electrodes	Acceleration direction interval θ(°)
1	1(x), 2(x)	$0<\theta<30°$
2	1(x), 2(x),1(y)	$15°<\theta< 45°$
3	1(x), 2(x),1(y), 2(y)	$30°<\theta<60°$
4	1(x), 1(y), 2(y)	$45°<\theta<75°$
5	1(y), 2(y)	$60°<\theta<90°$

5. Conclusion

An inertial micro-switch with three threshold values has been successfully designed, simulated, fabricated, and tested. The device consists of twelve stationary electrodes with a proof mass that holds four movable electrodes. The acceleration direction interval is determined by Contact-electrodes. The resolution and accuracy of the acceleration magnitude and direction increases with the number of threshold levels. Correspondingly for a higher number of bits, it can provide more precise acceleration direction information. A drop table system was used to test the fabricated inertial switch. The test results are consistent with the simulated ones. In conclusion, the designed switch is capable of detecting the acceleration thresholds as well as acceleration direction intervals.

REFERENCES

[1] C. Ren, K. Wang, P. Zhang, Y. Li, Z. Zhao, X. Shi, & Z. Yang, "A Self-Powered MEMS Inertial Switch for Potential Zero Power-Consumption Wake-Up Application," *J. Microelectromech. Syst.*, vol. 30, no. 4, pp. 550-559, May. 2021.

[2] I. J. Lee, Y. Song, H. Jung, J. Choi, Y. Eun & J. Kim, "Deformable carbon nanotube-contact pads for inertial microswitch to extend contact time," *IEEE Trans. Ind. Electron.,* vol. 59, no. 12, pp.4914-4920, Aug. 2011.

[3] L. J. Currano, C. R. Becker, G. L. Smith, B. Isaacson, & C. J. Morris, "3-axis acceleration switch for traumatic brain injury early warning," in *2012 IEEE 25th International Conference on Micro Electro Mechanical Systems (MEMS)*, DOI: 10.1109/MEMSYS.2012.6170229 pp. 484-487, Jan. 2012.

[4] Q. Xu, Z. Yang, Y. Sun, L. Lai, Z. Jin, G. Ding, X. Zhao, J. Yao, J. Wang, "Shock-resistibility of mems-based inertial microswitch under reverse directional ultra-high g acceleration for IoT applications," *Sci. Rep.*, vol. 7, no. 1, pp. 1-12, Mar. 2017.

[5] Y. Cao, Z. Xi, P. Yu, J. Wang, & W. Nie, "Optical measurement of the dynamic contact process of a MEMS inertial switch under high shock loads," *IEEE Trans. Ind. Electron.,* vol. 64, no. 1, pp.701-709, Sep. 2016.

[6] M. Liu, Y. Zhu, C. Wang, Y. Chen, Y. Wu, H. Zhang, & W. Wang, "A novel low-g MEMS bistable inertial switch with self-locking and reverse-unlocking functions," *J. Microelectromech. Syst.*, vol. 29, no. 6, pp. 1493-1503, Oct. 2020.

[7] S. Michaelis, H. J. Timme, M. Wycisk, & J. Binder, "Additive electroplating technology as a post-CMOS process for the production of MEMS acceleration-threshold switches for transportation applications," *J. Micromech. Microeng*., vol. 10, no. 2, pp.120-123, Jun. 2000.

[8] L. Du, Y. Li, J. Zhao, W. Wang, W. Zhao, W. Zhao, & H. Zhu, "A low-g MEMS inertial switch with a novel radial electrode for uniform omnidirectional sensitivity," *Sens. Actuators A*, vol. 270, pp. 214-222, Feb. 2018.

[9] X. Zhang, X. Xiang, Y. Wang, G. Ding, X. Xu, & Z. Yang, "A Heterogeneous Integrated MEMS Inertial Switch With Compliant Cantilevers Fixed Electrode and Electrostatic Locking to Realize Stable On-State," *J. Microelectromech Syst.*, vol. 28, no. 6, pp. 977-986, Sep. 2019.

[10] H.M. Ouakad, M.I. Younis, F. Alsaleem, "Dynamic response of an electrostatically actuated microbeam to drop-table test," *J. Micromech. Microeng*., vol. 22, no. 9, Jul. 2012, Art. no.095003.

[11] P. Zhang, Y. Li, C. Ren, H. Zhang, X. Shi, Y. Liu, & Z. Yang, "A MEMS Inertial Switch With Large Scale Bi-Directional Adjustable Threshold Function," *J. Microelectromech Syst.*, vol. 31, no. 1, pp. 124-133, Nov. 2021.

[12] J.C. Kuo, P.H. Kuo, Y.T. Lai, et al., "A passive inertial switch using MWCNT-hydrogel composite with wireless interrogation capability, " *J. Microelectromech Syst.*, vol. 22, no. 3, pp. 646-654, Jan. 2013.

[13] S. Michaelis, H.J. Timme, M. Wycisk, J. Binder, "Acceleration threshold switches from an additive electroplating MEMS process," *Sens. Actuators A*, vol. 85, no. 1-3, pp. 418-423, Aug. 2000.

[14] M.I. Younis, F.M. Alsaleem, R. Miles, Q. Su, "Characterization of the performance of capacitive switches activated by mechanical shock," *J. Micromech. Microeng*., vol. 17, no. 7, pp.1360-1370, Jun. 2007.

[15] C.W.Ma, P.C.Huang, J.C.Kuo, et al., "A novel inertial switch with an adjustable acceleration threshold using an MEMS digital-to-analog converter," *Microelectron Eng.*, vol. 110 pp. 374-380, Oct. 2013.

[16] F. Zhang, C. Wang, M. Yuan, B.Tang, & Z. Xiong, "Conception, fabrication and characterization of a silicon based MEMS inertial switch with a threshold value of 5 g," *J. Micromech. Microeng*., vol. 27, no. 12, Oct. 2017, Art. no. 125001.

[17] Z. Xiong, C. Wang, F. Zhang, J. Xie, Z. Shen, & B. Tang, "A Low-g MEMS Inertial Switch Based on Direct Contact Sensing Method," *IEEE. Trans. Compon. Packaging Manuf. Technol.*, vol. 9, no. 8, pp. 1535-1541, Jul. 2019.

[18] Q. Xu, B. Sun, Y. Li, X. Xiang, L. Lai, J. Li, G. Ding, X. Zhao, Z. Yang, "Design and characterization of an inertial microswitch with synchronous follow-up flexible compliant electrodes capable of extending contact duration," *Sens. Actuators A*, vol. 270, pp. 34-45, Feb. 2018.

[19] V. Singh, V. Kumar, A. Saini, P. K. Khosla, & S. Mishra, "Design and Development of the MEMS-Based High-g Acceleration Threshold Switch," *J. Microelectromech. Syst.*, vol. 30, no. 1, pp. 24-31, Nov. 2020.

[20] Q. Xu, Z.Q. Yang, B. Fu, Y.P. Bao, H. Wu, Y.N. Sun, M.Y. Zhao, J. Li, G.F. Ding, X. L. Zhao, "Design and Optimization of a stationary electrode in a vertically-driven mems inertial switch for extending contact duration," *Sensors*, vol. 17, no. 3, pp. 527-544, Mar. 2017.

[21] W. Chen, Z. Yang, Y. Wang, G. Ding, H. Wang, & X. Zhao, "Fabrication and characterization of a low-g inertial microswitch with flexible contact point and limit-block constraints," *IEEE ASME Trans. Mechatron.* vol. 21, no. 2, pp. 963-972, Aug. 2015.

[22] Q. Xu, Z. Yang, B. Fu, J. Li, H. Wu, Q. Zhang, Y. Sun, G. Ding, X. Zhao, "A surface-micromachining-based inertial micro-switch with compliant cantilever beam as movable electrode for enduring high shock and prolonging contact time," *Appl. Surf. Sci.*, vol. 387, pp. 569-580, Nov. 2016.

[23] A. Niyazi, Q. Xu, F. Khan, & M. I. Younis, Design, "Modeling, and Testing of a Bidirectional Multi-Threshold MEMS Inertial Switch," *Sens. Actuators A*, vol. 334, Feb. 2022, Art. no. 113219.

[24] R.R. Reddy, K. Komeda, Y. Okamoto, E. Lebrasseur, A. Higo, Y. Mita, "A zero-power sensing MEMS shock sensor with a latch-reset mechanism for multi-threshold events monitoring," *Sens. Actuators A*, vol. 295, pp. 1-10, Aug. 2019.

[25] Q. Xu, F. Khan, & M. I. Younis, "Multi-threshold inertial switch for quantitative acceleration measurements," IEEE Sens. J., vol. 21, no. 21 pp. 23849-23859, Sep. 2021.

[26] Z. Xi, N., Kong, W. Nie, Y. Cao, & C. Zheng, "High g MEMS inertial switch capable of direction detection," *Sens. Actuators A*, vol. 296, pp. 7-16, Sep. 2019.

[27] A. Post, T.B. Hoshizaki, M.D. Gilchrist, S. Brien, M. Cusimano, & S. Marshall, "Traumatic brain injuries: the influence of the direction of impact," *Neurosurgery*, vol. 76, no. 1, pp. 81-91, Jan. 2015.

[28] L. J. Currano, C. R. Becker, D. Lunking, G. L. Smith, B. Isaacson, & L. Thomas, "Triaxial inertial switch with multiple thresholds and resistive ladder readout," *Sens. Actuators A*, vol. 195, pp. 191-197, Jun. 2013.

[29] A. Ongkodjojo, & F. E Tay, "Optimized design of a micromachined G-switch based on contactless configuration for health care

applications," in *Journal of Physics: Conference Series* , vol. 34, no. 1, DOI:10.1088/1742-6596/34/1/173, pp. 1044-1052, Apr. 2006.

[30] R. Amarasinghe, D.V. Dao, T. Toriyama, S. Sugiyama, "Design & fabrication of piezoresistive six degree of freedom accelerometer for biomechanical applications," in *Proc. 2004 Int. Conf. MEMS, NANO and Smart Syst*, DOI**:** 10.1109/ICMENS.2004.1508936, pp. 148-154, Aug. 2004.

[31] H. Cai, Z. Yang, G. Ding, & X. Zhao, "Fabrication of a MEMS inertia switch on quartz substrate and evaluation of its threshold acceleration," *Microelectronics J.*, vol. 39, no. 9, pp. 1112-1119, Sep. 2008.

[32] ANSYS Inc.: www.ansys.com.

Qiu Xu received the B.Sc. degree from Jiangxi Normal University, Nanchang, China, in 2003. He received the M.Sc. degree from Shanghai Normal University, Shanghai, China, in 2007. He received the Ph.D. degree in microelectronics and solid state electronics at the National Key Laboratory of Science and Technology on Micro/Nano Fabrication, Shanghai Jiao Tong University, Shanghai, China, in 2017. He is currently a postdoctoral fellow at King Abdullah University of Science and Technology, Saudi Arabia. His research interests include the design, simulation, and fabrication of MEMS/NEMS devices.

Lvjun Wang received the B.Sc. degree from University of Science and Technology of China, Hefei, China in 2016 and the M.Sc. degree from King Abdullah University of Science and Technology, Thuwal, Saudi Arabia. He is currently a Ph.D. candidate with King Abdullah University of Science and Technology, Thuwal, Saudi Arabia. His research interests include fabrication, characterization, and dynamic analysis of MEMS and NEMS structures.

Mohammad I. Younis received a Ph.D. degree in engineering mechanics from Virginia Polytechnic Institute and State University in 2004. Since 2004, he has served as an assistant and then an associate professor of mechanical engineering at State University of New York at Binghamton. He is currently a Professor of Mechanical Engineering and the Director of the MEMS and NEMS Characterization and Motion Laboratory at King Abdullah University of Science and Technology, Saudi Arabia. Dr. Younis is a recipient of the SUNY Chancellor's Award for Excellence in Scholarship and Creative Activities in 2012, the National Science Foundation Faculty Early Career Development Award in 2009, and the Paul E. Torgersen Graduate Research Excellence Award in 2002. He holds several U.S. patents in MEMS sensors and actuators. He serves as an Associate Editor of Nonlinear Dynamics, the Journal of Computational and Nonlinear Dynamics, Meccanica, and the Journal of Vibration and Control. He is a member of the American Society of Mechanical Engineers and IEEE.